

Observation of a Superradiant Phase Transition with Emergent Cat States

Ri-Hua Zheng^{1,*}, Wen Ning^{1,*}, Ye-Hong Chen^{1,2,3,*}, Jia-Hao Lü¹, Li-Tuo Shen¹, Kai Xu^{4,5}, Yu-Ran Zhang^{6,2,3},
Da Xu⁷, Hekang Li⁵, Yan Xia¹, Fan Wu¹, Zhen-Biao Yang^{1,†}, Adam Miranowicz^{2,8}, Neill Lambert²,

Dongning Zheng^{4,5}, Heng Fan^{4,5}, Franco Nori^{2,3,9,‡} and Shi-Biao Zheng^{1,§}

¹*Fujian Key Laboratory of Quantum Information and Quantum Optics, College of Physics and Information Engineering, Fuzhou University, Fuzhou, Fujian 350108, China*

²*Theoretical Quantum Physics Laboratory, RIKEN Cluster for Pioneering Research, Wako-shi, Saitama 351-0198, Japan*

³*Quantum Information Physics Theory Research Team, RIKEN Center for Quantum Computing (RQC), Wako-shi, Saitama 351-0198, Japan*

⁴*Institute of Physics and Beijing National Laboratory for Condensed Matter Physics, Chinese Academy of Sciences, Beijing 100190, China*

⁵*CAS Center for Excellence in Topological Quantum Computation, University of Chinese Academy of Sciences, Beijing 100190, China*

⁶*School of Physics and Optoelectronics, South China University of Technology, Guangzhou 510640, China*

⁷*Interdisciplinary Center of Quantum Information, State Key Laboratory of Modern Optical Instrumentation and Zhejiang Province Key Laboratory of Quantum Technology and Device, School of Physics, Zhejiang University, Hangzhou 310027, China*

⁸*Institute of Spintronics and Quantum Information, Faculty of Physics, Adam Mickiewicz University, 61-614 Poznań, Poland*

⁹*Department of Physics, University of Michigan, Ann Arbor, Michigan 48109-1040, USA*



(Received 28 February 2023; revised 29 May 2023; accepted 10 August 2023; published 11 September 2023)

Superradiant phase transitions (SPTs) are important for understanding light-matter interactions at the quantum level, and play a central role in criticality-enhanced quantum sensing. So far, SPTs have been observed in driven-dissipative systems, but the emergent light fields did not show any nonclassical characteristic due to the presence of strong dissipation. Here we report an experimental demonstration of the SPT featuring the emergence of a highly nonclassical photonic field, realized with a resonator coupled to a superconducting qubit, implementing the quantum Rabi model. We fully characterize the light-matter state by Wigner matrix tomography. The measured matrix elements exhibit quantum interference intrinsic of a photonic mesoscopic superposition, and reveal light-matter entanglement.

DOI: [10.1103/PhysRevLett.131.113601](https://doi.org/10.1103/PhysRevLett.131.113601)

The Dicke model [1,2], involving a quantized light field coupled to N two-level atoms, represents a paradigm for realizing exotic quantum phenomena that are absent in semiclassical light-matter systems. Superradiant phase transitions (SPTs) are one of the most famous examples [3–5], where the behavior of the light is sharply changed when the light-matter coupling strength becomes comparable to their frequencies. Under equilibrium conditions, the SPT features a sudden buildup of a photonic field that is highly entangled with the atoms in a mesoscopic superposition [5]. In addition to its fundamental appeal, such cat states can be used as an intrinsically protected qubit for fault-tolerant quantum computation [6] and as a resource for quantum enhanced metrology [7]. The equilibrium SPT has been attracting enduring attention since the 1970s, but its experimental demonstration still remains very challenging. This is mainly because the neglected square of the vector potential actually increases quadratically with the coupling strength and the photon number, which prohibits the occurrence of SPTs, known as the no-go theorem [8]. Over the past decade, breakthrough experiments have been reported for dynamical realizations of SPTs with a collection of driven atoms trapped in an optical cavity [9–16],

whose photonic dissipation enabled the phase transition to be monitored by measuring the output field. This dissipation, however, at the same time obscured the quantum coherence of the light, as well as the light-matter entanglement inherent in the superradiant phase (SP).

Although originally proposed in the thermodynamic limit $N \rightarrow \infty$, SPTs can actually occur in the quantum Rabi model (QRM), which only involves a single atom coupled to a light field [17,18]. Recent years have witnessed remarkable advances in simulations of the Rabi model in different systems, where the photonic mode was emulated by a phononic mode of a trapped ion [19,20], while the light field coupling the ion's internal and external degrees of freedom is classical. Circuit QED represents an alternative excellent platform for exploring quantized light-matter systems in regimes that are inaccessible with conventional cavity QED [21–24], and for simulating controlled many-body dynamics [25,26]. In particular, recent experiments [27] have demonstrated some spectroscopic signatures in the deep-strong coupling regimes. The long coherence times of the superconducting qubits and the microwave photons makes circuit QED promising for realizing SPT produced by a unitary process, in distinct

contrast with ultracold-atoms-based cavity QED systems [9–16], where SPT was realized in a dissipative-driven manner. This unitary nature, together with the ability to individually control and measure the superconducting qubits, enables the exploration of nonclassical characteristics associated with the SPT, such as the qubit-resonator entanglement and phase-space quantum interference behaviors of the resonator.

Theoretical investigations indicate that the no-go theorem can be circumvented in circuit QED systems [28]. However, the approximation for describing a superconducting artificial atom as a qubit may break down when increasing the coupling strength due to the limited anharmonicity [29], which prohibits the occurrence of dynamical signatures of the Rabi model, even when the deep-strong regime is reached [27]. To overcome this problem, it was proposed to effectively transform the Jaynes-Cummings model into the Rabi model, by applying continuous microwave fields to the qubit [22,30] or by introducing a two-photon drive to the resonator [31–34]. Following these approaches, some important features predicted by the Rabi model have been observed [35,36]. Despite these advancements, so far the SPT of a real radiant field with nonclassical features has not been reported in any system.

Here we report a realization of the first-order SPT of a quantum light field manifested by an emergent cat state. Our demonstration involves a resonator and a superconducting qubit coupled at the second sideband of a strong parametric modulation produced by an ac magnetic flux. This strong longitudinal modulation, together with a weak modulation and a transverse microwave driving, enables the realization of an effective Rabi model with a controllable coupling-frequency ratio. We fully describe the nonclassical behavior of the system by measuring the Wigner

function matrix of the joint qubit-resonator system, which contains full information about its state. The measured matrix elements unambiguously demonstrate that the photonic field emergent in the SP is in a quantum superposition of two quasiclassical states that are degenerate in amplitude but have opposite phases. These results bridge the gap between the phase transitions predicted in closed quantum systems and those observed in real macroscopic systems, which is critical to understanding how a symmetry-broken macroscopic order emerges from the dynamics governed by a symmetry-preserving Hamiltonian.

The theoretical model includes a quantized light field stored in a resonator coupled to a qubit, e.g., a tunable Xmon qubit [see Fig. 1(a)], whose transition frequency is periodically modulated [37] as $\omega_q = \omega_0 + \varepsilon_1 \cos(\nu_1 t) + \varepsilon_2 \cos(\nu_2 t)$, where ω_0 corresponds to the mean transition frequency of the qubit, and $\varepsilon_{1,(2)}$ [$\nu_{1,(2)}$] are the corresponding modulation amplitudes (frequencies). In addition to these longitudinal modulations, the qubit is transversely driven by an external field at the frequency ω_0 with an amplitude K . The system dynamics is described by the Hamiltonian

$$H = \hbar \left[\omega_p a^\dagger a + \frac{\omega_q}{2} \sigma_z + (\lambda a^\dagger \sigma_- + K e^{i\omega_0 t} \sigma_- + \text{H.c.}) \right], \quad (1)$$

where a^\dagger (a) denotes the creation (annihilation) operator for the photonic field with frequency ω_p , λ is the qubit-resonator coupling strength, $\sigma_z = |e\rangle\langle e| - |g\rangle\langle g|$, and $\sigma_- = |g\rangle\langle e|$ are Pauli operators for the qubit. Under the condition $\nu_1 \gg \lambda, K, \delta$ with $\delta = \omega_p - \omega_0 - 2\nu_1$, the resonator interacts with the qubit at the second sideband associated with

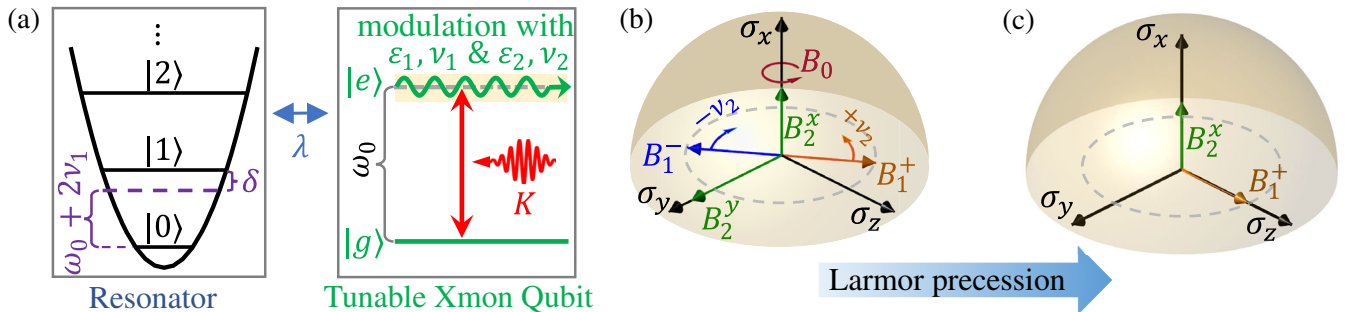


FIG. 1. Theoretical model. (a) Sketch for the qubit-resonator coupling. The test qubit is coupled to the resonator at the second sideband of a sine longitudinal modulation with modulating amplitude ε_1 and frequency ν_1 . A second sine modulation with amplitude ε_2 and frequency ν_2 is used to control the effective frequency of the qubit. These two modulations, together with a transverse drive K , effectively realizes an effective Rabi Hamiltonian. Bloch representations in (b) the laboratory frame and (c) the precessing frame. By analogy with the motion of a spin-1/2, the transverse drive can be regarded as a static magnetic field of strength $B_0 \propto K$ along the x axis, which forces the Bloch vector of the qubit to precess with angular frequency B_0 . The second longitudinal modulation corresponds to applying two magnetic fields on the yz plane with the same amplitude $|B_1^\pm| = \varepsilon_2/4$, rotating at the same angular frequency $\nu_2 = B_0$, but in opposite directions. The light field stored in the resonator acts as an effective magnetic field with components B_2^x and B_2^y . In the precessing frame associated with B_0 , the components B_1^+ and B_2^x are aligned with the z and x axes, respectively. The remaining components have negligible effects in the rotating-wave approximation (not shown).

the first modulation, while the drive works at the carrier, as shown in Fig. 1(a).

The effective dynamics can be well understood in terms of the motion of a spin-1/2 in magnetic fields. As shown in Fig. 1(b), the transverse drive can be thought of as a static magnetic field of strength $B_0 = 2KJ_0(\mu)$ along the x axis, forcing the Bloch vector of the qubit to make a Larmor precession with angular frequency B_0 , where $J_m(\mu)$ denotes the m th Bessel function of the first kind with $\mu = \varepsilon_1/\nu_1$. The second longitudinal modulation acts as the combination of two components: B_1^\pm that have the same amplitude $|B_1^\pm| = \varepsilon_2/4$, but rotate with opposite angular velocities $\pm\nu_2$ on the yz plane. On the other hand, the quantized light field behaves like a magnetic field with the x and y components

$$B_2^x = 2\eta(a + a^\dagger), \quad B_2^y = 2i\eta(a^\dagger - a), \quad (2)$$

where $\eta = \lambda J_2(\mu)/2$. When $B_0 = \nu_2 \gg B_1, B_2^{x(y)}$, in the framework coinciding with the Larmor precession, the components B_1^- and B_2^y can be discarded due to fast rotations [see Fig. 1(c)]. Consequently, the dynamics can be described by the effective quantum Rabi Hamiltonian ($\hbar = 1$)

$$H_R = \frac{1}{2}\Omega\sigma_z + \delta a^\dagger a + \eta\sigma_x(a + a^\dagger), \quad (3)$$

which is obtained by subsequently performing the transformations $\exp[i\int_0^t H_0 dt]$ and $\exp(iB_0\sigma_x t/2)$ and

neglecting the fast-oscillating terms (see Supplemental Material, Sec. S1 A [38]), where $\Omega = \varepsilon_2/2$ and

$$H_0 = (\omega_0 + 2\nu_1)a^\dagger a + \frac{1}{2}[\omega_0 + \varepsilon_1 \cos(\nu_1 t)]\sigma_z. \quad (4)$$

We note that the synthesized qubit-resonator system corresponds to an isomorphism of the QRM [52], where the effective counterrotating-wave coupling is produced by the external drive, but not inherent in the qubit-resonator interaction as in the QRM without driving. With this realization, the system frequencies are replaced by the transverse driving detuning and the longitudinal modulation amplitude, which can be easily tuned. Consequently, the critical point of the SPT can be reached in the effective QRM without requiring the qubit-resonator coupling to be comparable to the system frequencies, thereby circumventing the restriction of the no-go theorem.

Our experimental device possesses a bus resonator and five frequency-tunable Xmon qubits, one of which is used as the test qubit for realizing the QRM. Before the experiment, each qubit is initialized to its ground state. The experiment starts by tuning the test qubit to the operating frequency $\omega_0/2\pi = 5.18$ GHz, where a continuous microwave K is applied. This transverse driving, together with the two longitudinal sine modulations, effectively realizes the Rabi Hamiltonian of Eq. (3). The experimental details are shown in Supplemental Material, Sec. S2 [38], including experimental setup, device parameters, and pulse sequence. During the quenching process where the ratio $\xi = 2\eta/\sqrt{\Omega\delta}$ is slowly increased,

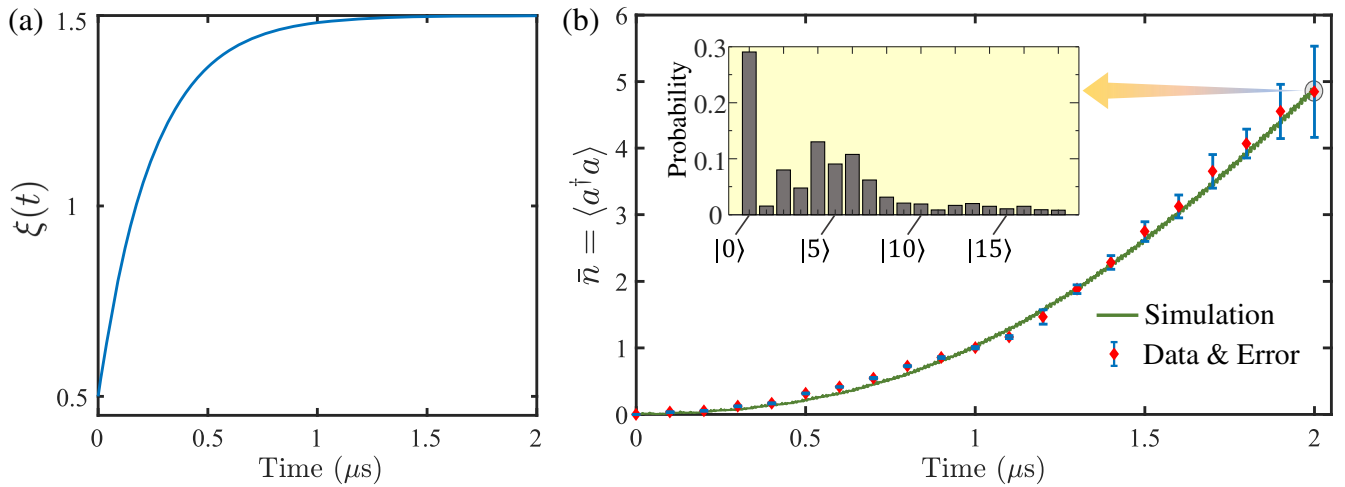


FIG. 2. (a) Control parameter $\xi(t)$ versus time t . During the quenching process, the effective frequencies of the qubit and the resonator are respectively varied as $\Omega = 2\sqrt{10}\eta/[1.5 - \exp(-8t/t_f)]$ and $\delta \simeq \Omega/10$, with $t_f = 2 \mu\text{s}$, while the effective coupling strength is fixed to $\eta/2\pi = 0.81$ MHz. Experimentally, Ω is controllable by ε_2 , and δ is adjustable by the Stark shift produced by an ancilla qubit dispersively coupled to the resonator. With these settings, $\xi(t)$ depends on t as $\xi(t) = 1.5 - \exp(-8t/t_f)$. (b) Observed dynamical evolution of the average photon number $\bar{n} = \langle a^\dagger a \rangle$. The green curve shows the result of numerical simulation based on the master equation, where the parameters of the control fields are set to $K/(2\pi) = 19.9$, $\varepsilon_1/(2\pi) = 165.85$, $\nu_1/(2\pi) = 200$, $\nu_2/(2\pi) = 33.28$ MHz, and $\varepsilon_2 = 3.08\Omega$, and the qubit and resonator frequencies are $\omega_0/(2\pi) = 5.18$ GHz and $\omega_p = \omega_0 + 2\nu_1 + \delta$, respectively. The relaxation time T_1 (dephasing time T_2^*) for the qubit and the resonator are 21.5 and 12.9 μs (1.1 and 234.5 μs), respectively, each measured in independent experiments. The inset shows the photon number distribution of the resonator measured at $t = 2 \mu\text{s}$.

all the qubits, except the test one, remain in their ground states as they are detuned from the resonator by an amount about twenty times larger than the corresponding qubit-resonator coupling strengths. Such a process is realized by varying the control parameter as $\xi(t) = 1.5 - \exp(-8t/t_f)$, with $t_f = 2 \mu\text{s}$.

To characterize the photon-number populations after a preset quench time, the microwave drive and the frequency modulations are switched off, so that the test qubit is effectively decoupled from the resonator since the detuning between the qubit and the resonator is 20 times their coupling strength without modulations. Subsequently, an ancilla qubit is tuned on resonance with the resonator, undergoing photon-number-dependent Rabi oscillations. The photonic populations of the resonator can be inferred from the measured Rabi oscillations signals [53]. Figure 2 shows the measured average photon number ($\bar{n} = \langle a^\dagger a \rangle$) versus time. We compare the measured values with the theoretical predictions and show that the experimental result agrees well with the simulation.

The exotic behavior in the SP can be characterized by the Wigner function matrix that contains full information about the joint qubit-resonator state [54]. In terms of the qubit basis $\{|g\rangle, |e\rangle\}$, the density operator is expressed as

$$\rho = \sum_{k=g,e} \sum_{k'=g,e} \rho_{k,k'} \otimes |k\rangle\langle k'|, \quad (5)$$

with $\rho_{k,k'} = \langle k|\rho|k'\rangle$ matrix elements.

The information of the element $\rho_{k,k'}$ is contained in the corresponding Wigner matrix element $W_{k,k'}(\beta)$. To measure the Wigner matrix elements, we translate in phase space the resonator state by β . The matrix elements are inferred by measuring the test qubits along three mutual axes, and correlating the outcomes to the photon number distributions of the resonator measured with the ancilla qubit (see Supplemental Material, Sec. S5 [38] for detailed characterization of the qubit-resonator state). Figures 3(a)–3(d) show the Wigner matrix elements reconstructed at $t = 1.946 \mu\text{s}$, which reveal that the field exhibits two quasiclassical components with the same amplitude but opposite phases $|\pm\alpha\rangle$ and a vacuum component, featuring a first-order phase transition. The strong quantum coherence between the “empty” state $|0\rangle$ and “filled” states $|\pm\alpha\rangle$, distinguishes this SPT from the first-order phase transition previously investigated in the Dicke model with the mean field description [15,33,55]. The resulting output state can be regarded as a super-cat state, featuring being simultaneously empty and filled, where the filled state itself is a cat state composed of the two components $|\pm\alpha\rangle$ superimposed with each other. This super-cat state is significantly distinct from the ground state of the ideal Rabi model with an infinite frequency ratio [18], in which the population of the vacuum component tends to 0. As shown in Fig. S7 of the Supplemental Material [38], Sec. S4, the limitation of the effective frequency ratio, nonadiabaticity, and deviation from model Hamiltonian contribute vacuum populations of 0.04, 0.03, 0.06,

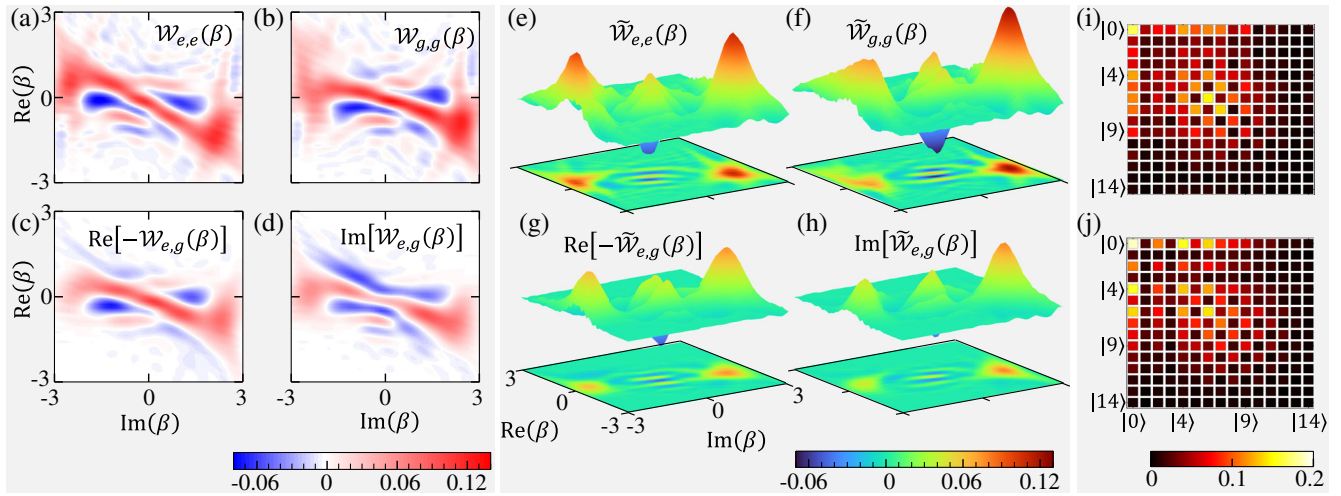


FIG. 3. Wigner matrix tomography. (a)–(d) Measured matrix elements for the super-cat state. The value of the matrix elements at each point is reconstructed from the Wigner diagonal elements measured along the three mutually orthogonal axes of the Bloch sphere of the qubit. Each of these diagonal elements is obtained from the measured photon number distribution of the field displaced by β in phase space, correlated with detection of the test qubit along the corresponding axis. All the data are measured at $t = 1.946 \mu\text{s}$. (e)–(h) Matrix elements for the superradiant-phase cat state. These Wigner matrix elements are extracted by reconstructing the qubit-resonator density matrix in the Fock basis, discarding the elements associated with $|0\rangle$ to obtain system density matrix associated with the superradiant phase, from which the corresponding Wigner matrix is obtained. The inferred vacuum population in the superradiant phase is $\sim 0.1\%$, which implies that the measured vacuum population of about 30% mainly arises from the normal phase that coexists with the superradiant phase. (i),(j) Normalized density matrices of the resonator associated with the qubit states $|e\rangle$ and $|g\rangle$. For clarity, we here only display the magnitudes of the elements.

respectively. The dissipation is responsible for the rest of vacuum population (~ 0.16), and turns the qubit-resonator system into a partially mixed state, with a purity of $\text{Tr}(\rho^2) = 0.46$. With the increase of the distance from the critical point, the size of the cat state would be improved at the price of degradation of the state purity, as a consequence of its increasing sensitivity to dissipation and the longer time needed for the quenching process.

To further confirm this exotic phenomenon, we separate the measured coherent fields with amplitude $|\alpha|$ from the vacuum field, enabled by their large distance in phase space. The extracted Wigner matrix elements for the SP are displayed in Figs. 3(e)–3(h). As expected, each of these elements exhibits two peaks, between which there exists an oscillating pattern featuring the alternating appearance of positive and negative values, as a consequence of quantum interference between $|\pm\alpha\rangle$ [56]. The distortions of the Gaussian peaks are mainly due to the neglected high-order nonlinear processes and the limited frequency ratio $\Omega/\delta \simeq 10$. These results unambiguously demonstrate that the photons produced in the SP spontaneously form a catlike state. For each of the two quasiclassical components forming the cat state, the parity symmetry is broken. The extent of the symmetry breaking is quantified by the field coherence, $\langle a \rangle$, which is equal to the amplitude of the quasiclassical coherent state and can be used as an order parameter to characterize the QPT [18,57].

After the quenching dynamics, this coherence has a magnitude of 2.62, which indicates the occurrence of a phase transition during the quenching process [58]. The resulting cat state formed by two coherent states $|\pm\alpha\rangle$ has a size of $d^2 = 4|\alpha|^2 = 27.46$ [56]. The inferred diagonal element $\tilde{\mathcal{W}}_{e,e}$ ($\tilde{\mathcal{W}}_{g,g}$) has a minimum value of -0.060 (-0.068) at $\beta = -0.48 - 0.36i$ ($\beta = -0.48i$). These negative phase-space quasi-probability densities show the nonclassicality of the emergent photonic field. The photon-matter entanglement can be quantified by using the negativity obtained from the partially transposed density matrix [59]. The negativity for the SP, inferred from the qubit-resonator density matrix associated with the SP, is 0.12, which confirms the existence of strong light-matter entanglement, making the present SP distinct from those realized in previous experiments [9–16], where no entanglement was observed due to the strong decoherence. Because of the decoherence effects, this negativity is smaller than that for the ideal superradiant ground state, which has a value of 0.44.

The quantum coherence between the coexisting phases can be further confirmed by the off-diagonal elements between $|0\rangle$ and $|n\rangle$ ($n \neq 0$) in the Fock basis associated with $\mathcal{W}_{e,e}$ and $\mathcal{W}_{g,g}$, displayed in Figs. 3(i) and 3(j). The coherences between the empty state and filled state, defined as $C_{k,k} = \sum_{n \neq 0} |\langle 0|\rho_{k,k}|n\rangle|/\text{Tr}(\rho_{k,k})$, are 1.018 and 1.020 for the renormalized resonator density matrices correlated with $|e\rangle$ and $|g\rangle$, respectively. Each of these coherences is

much larger than that of the coherent state $|\alpha\rangle$, $C_\alpha = \sum_{n \neq 0} |\langle 0|\alpha\rangle\langle\alpha|n\rangle| = 0.1147$, which verifies that these coherences are mainly due to the quantum superposition between the SP and the normal phase. The negativity of the realized first-order phase transition is 0.25, which quantifies the qubit-resonator of the output density matrix, reconstructed without removing the elements associated with the vacuum state component $|0\rangle$. This negativity is significantly higher than that for the SP, mainly due to the fact that the vacuum state is not subjected to decoherence.

In conclusion, we have theoretically proposed and experimentally demonstrated a method for exploring the SPT of a microwave photonic field stored in a resonator coupled to a superconducting artificial atom. The reconstructed resonator-qubit Wigner matrix reveals quantum interference effects between the vacuum and the SP cat states, and between the two SP states, as well as light-matter entanglement. It is expected that the emergent cat state loses its coherence at an increasing rate with the increase of the photon number, as a consequence of the information acquisition about the phase or amplitude of the field by the environment. Progressively increasing the quench parameter would make it possible to experimentally explore the intimate relation between the symmetry breaking process and decoherence, which plays a central role in the quantum-to-classical transition. In addition to fundamental interest, our system may find applications in quantum technology.

We acknowledge helpful discussions with Anton Frisk Kockum. This work was supported by the National Natural Science Foundation of China (Grants No. 12274080, No. 11875108, No. 11934018, No. 11904393, No. 92065114, and No. T2121001), Innovation Program for Quantum Science and Technology under Grant No. 2021ZD0300200, the Strategic Priority Research Program of Chinese Academy of Sciences (Grant No. XDB28000000), the Key-Area Research and Development Program of Guangdong Province, China (Grant No. 2020B0303030001), the Natural Science Funds for Distinguished Young Scholar of Fujian Province under Grant 2020J06011, Projects from Fuzhou University under Grants No. JG202001-2 and No. 049050011050, and Beijing Natural Science Foundation (Grant No. Z200009). A. M. is supported by the Polish National Science Centre (NCN) under the Maestro Grant No. DEC-2019/34/A/ST2/00081. F. N. is supported in part by: Nippon Telegraph and Telephone Corporation (NTT) Research, the Japan Science and Technology Agency (JST) [via the Quantum Leap Flagship Program (Q-LEAP), and the Moonshot R&D Grant No. JPMJMS2061], the Asian Office of Aerospace Research and Development (AOARD) (via Grant No. FA2386-20-1-4069), and the Foundational Questions Institute Fund (FQXi) via Grant No. FQXi-IAF19-06.

*These authors contribute equally to this work.

†zbyang@fzu.edu.cn

‡fnori@riken.jp

§t96034@fzu.edu.cn

- [1] R. H. Dicke, Coherence in spontaneous radiation processes, *Phys. Rev.* **93**, 99 (1954).
- [2] P. Kirton, M. M. Roses, J. Keeling, and E. G. Dalla Torre, Introduction to the Dicke model: From equilibrium to nonequilibrium, and vice versa, *Adv. Quantum Technol.* **2**, 1800043 (2019).
- [3] Y. K. Wang and F. T. Hioe, Phase transition in the Dicke model of superradiance, *Phys. Rev. A* **7**, 831 (1973).
- [4] K. Hepp and E. H. Lieb, On the superradiant phase transition for molecules in a quantized radiation field: The Dicke maser model, *Ann. Phys. (N.Y.)* **76**, 360 (1973).
- [5] N. Lambert, C. Emary, and T. Brandes, Entanglement and the Phase Transition in Single-Mode Superradiance, *Phys. Rev. Lett.* **92**, 073602 (2004).
- [6] P. Nataf and C. Ciuti, Protected Quantum Computation with Multiple Resonators in Ultrastrong Coupling Circuit QED, *Phys. Rev. Lett.* **107**, 190402 (2011).
- [7] H. Kwon, K. C. Tan, T. Volkoff, and H. Jeong, Non-classicality as a Quantifiable Resource for Quantum Metrology, *Phys. Rev. Lett.* **122**, 040503 (2019).
- [8] K. Rzażewski, K. Wódkiewicz, and W. Żakowicz, Phase Transitions, Two-Level Atoms, and the A^2 Term, *Phys. Rev. Lett.* **35**, 432 (1975).
- [9] Z. Zhang, C. H. Lee, R. Kumar, K. J. Arnold, S. J. Masson, A. S. Parkins, and M. D. Barrett, Nonequilibrium phase transition in a spin-1 Dicke model, *Optica* **4**, 424 (2017).
- [10] K. Baumann, C. Guerlin, F. Brennecke, and T. Esslinger, Dicke quantum phase transition with a superfluid gas in an optical cavity, *Nature (London)* **464**, 1301 (2010).
- [11] K. Baumann, R. Mottl, F. Brennecke, and T. Esslinger, Exploring Symmetry Breaking at the Dicke Quantum Phase Transition, *Phys. Rev. Lett.* **107**, 140402 (2011).
- [12] F. Brennecke, R. Mottl, K. Baumann, R. Landig, T. Donner, and T. Esslinger, Real-time observation of fluctuations at the driven-dissipative Dicke phase transition, *Proc. Natl. Acad. Sci. U.S.A.* **110**, 11763 (2013).
- [13] J. Klinder, H. Keßler, M. Wolke, L. Mathey, and A. Hemmerich, Dynamical phase transition in the open Dicke model, *Proc. Natl. Acad. Sci. U.S.A.* **112**, 3290 (2015).
- [14] J. Léonard, A. Morales, P. Zupancic, T. Esslinger, and T. Donner, Supersolid formation in a quantum gas breaking a continuous translational symmetry, *Nature (London)* **543**, 87 (2017).
- [15] F. Ferri, R. Rosa-Medina, F. Finger, N. Dogra, M. Soriente, O. Zilberberg, T. Donner, and T. Esslinger, Emerging Dissipative Phases in a Superradiant Quantum Gas with Tunable Decay, *Phys. Rev. X* **11**, 041046 (2021).
- [16] X. Zhang, Y. Chen, Z. Wu, J. Wang, J. Fan, S. Deng, and H. Wu, Observation of a superradiant quantum phase transition in an intracavity degenerate Fermi gas, *Science* **373**, 1359 (2021).
- [17] S. Ashhab, Superradiance transition in a system with a single qubit and a single oscillator, *Phys. Rev. A* **87**, 013826 (2013).
- [18] M.-J. Hwang, R. Puebla, and M. B. Plenio, Quantum Phase Transition and Universal Dynamics in the Rabi Model, *Phys. Rev. Lett.* **115**, 180404 (2015).
- [19] D. Lv, S. An, Z. Liu, J.-N. Zhang, J. S. Pedernales, L. Lamata, E. Solano, and K. Kim, Quantum Simulation of the Quantum Rabi Model in a Trapped Ion, *Phys. Rev. X* **8**, 021027 (2018).
- [20] M.-L. Cai, Z.-D. Liu, W.-D. Zhao, Y.-K. Wu, Q.-X. Mei, Y. Jiang, L. He, X. Zhang, Z.-C. Zhou, and L.-M. Duan, Observation of a quantum phase transition in the quantum Rabi model with a single trapped ion, *Nat. Commun.* **12**, 1126 (2021).
- [21] A. F. Kockum, A. Miranowicz, S. D. Liberato, S. Savasta, and F. Nori, Ultrastrong coupling between light and matter, *Nat. Rev. Phys.* **1**, 19 (2019).
- [22] P. Form-Díaz, L. Lamata, E. Rico, J. Kono, and E. Solano, Ultrastrong coupling regimes of light-matter interaction, *Rev. Mod. Phys.* **91**, 025005 (2019).
- [23] X. Gu, A. F. Kockum, A. Miranowicz, Y.-X. Liu, and F. Nori, Microwave photonics with superconducting quantum circuits, *Phys. Rep.* **718–719**, 1 (2017).
- [24] D. Ballester, G. Romero, J. J. García-Ripoll, F. Deppe, and E. Solano, Quantum Simulation of the Ultrastrong-Coupling Dynamics in Circuit Quantum Electrodynamics, *Phys. Rev. X* **2**, 021007 (2012).
- [25] M. Feng, Y. P. Zhong, T. Liu, L. L. Yan, W. L. Yang, J. Twamley, and H. Wang, Exploring the quantum critical behaviour in a driven Tavis-Cummings circuit, *Nat. Commun.* **6**, 7111 (2015).
- [26] K. Xu, Z.-H. Sun, W. Liu, Y.-R. Zhang, H. Li, H. Dong, W. Ren, P. Zhang, F. Nori, D. Zheng, H. Fan, and H. Wang, Probing dynamical phase transitions with a superconducting quantum simulator, *Sci. Adv.* **6**, eaba4935 (2020).
- [27] F. Yoshihara, T. Fuse, Z. Ao, S. Ashhab, K. Kakuyanagi, S. Saito, T. Aoki, K. Koshino, and K. Semba, Inversion of Qubit Energy Levels in Qubit-Oscillator Circuits in the Deep-Strong-Coupling Regime, *Phys. Rev. Lett.* **120**, 183601 (2018).
- [28] P. Nataf and C. Ciuti, No-go theorem for superradiant quantum phase transitions in cavity QED and counterexample in circuit QED, *Nat. Commun.* **1**, 72 (2010).
- [29] D. De Bernardis, P. Pilar, T. Jaako, S. De Liberato, and P. Rabl, Breakdown of gauge invariance in ultrastrong-coupling cavity QED, *Phys. Rev. A* **98**, 053819 (2018).
- [30] C. Sánchez Muñoz, A. Frisk Kockum, A. Miranowicz, and F. Nori, Simulating ultrastrong-coupling processes breaking parity conservation in Jaynes-Cummings systems, *Phys. Rev. A* **102**, 033716 (2020).
- [31] W. Qin, A. Miranowicz, P.-B. Li, X.-Y. Lü, J. Q. You, and F. Nori, Exponentially Enhanced Light-Matter Interaction, Cooperativities, and Steady-State Entanglement using Parametric Amplification, *Phys. Rev. Lett.* **120**, 093601 (2018).
- [32] C. Leroux, L. C. G. Govia, and A. A. Clerk, Enhancing Cavity Quantum Electrodynamics via Antisqueezing: Synthetic Ultrastrong Coupling, *Phys. Rev. Lett.* **120**, 093602 (2018).
- [33] C. J. Zhu, L. L. Ping, Y. P. Yang, and G. S. Agarwal, Squeezed Light Induced Symmetry Breaking Superradiant Phase Transition, *Phys. Rev. Lett.* **124**, 073602 (2020).

- [34] Y.-H. Chen, W. Qin, X. Wang, A. Miranowicz, and F. Nori, Shortcuts to Adiabaticity for the Quantum Rabi Model: Efficient Generation of Giant Entangled Cat States via Parametric Amplification, *Phys. Rev. Lett.* **126**, 023602 (2021).
- [35] N. K. Langford, R. Sagastizabal, M. Kounalakis, C. Dickel, A. Bruno, F. Luthi, D. J. Thoen, A. Endo, and L. DiCarlo, Experimentally simulating the dynamics of quantum light and matter at deep-strong coupling, *Nat. Commun.* **8**, 1715 (2017).
- [36] J. Braumüller, M. Marthaler, A. Schneider, A. Stehli, H. Rotzinger, M. Weides, and A. V. Ustinov, Analog quantum simulation of the Rabi model in the ultra-strong coupling regime, *Nat. Commun.* **8**, 779 (2017).
- [37] D.-W. Wang, C. Song, W. Feng, H. Cai, D. Xu, H. Deng, H. Li, D. Zheng, X. Zhu, H. Wang, S.-Y. Zhu, and M. O. Scully, Synthesis of antisymmetric spin exchange interaction and chiral spin clusters in superconducting circuits, *Nat. Phys.* **15**, 382 (2019).
- [38] See Supplemental Material at <http://link.aps.org/supplemental/10.1103/PhysRevLett.131.113601> for a derivation of the effective Rabi Hamiltonian, a description of the system parameters, experimental pulse sequences, quenching dynamics, and techniques for characterizing the qubit-resonator output states, a discussion of experimental imperfections, including the limitation of the effective frequency ratio, nonadiabaticity, dissipation, and deviations from the ideal Hamiltonian, as well as a numerical simulation of the superradiant phase transition in the Dicke model, which includes Refs. [39–51].
- [39] C. Song, S.-B. Zheng, P. Zhang, K. Xu, L. Zhang, Q. Guo, W. Liu, D. Xu, H. Deng, K. Huang, D. Zheng, X. Zhu, and H. Wang, Continuous-variable geometric phase and its manipulation for quantum computation in a superconducting circuit, *Nat. Commun.* **8**, 1061 (2017).
- [40] W. Ning, X.-J. Huang, P.-R. Han, H. Li, H. Deng, Z.-B. Yang, Z.-R. Zhong, Y. Xia, K. Xu, D. Zheng, and S.-B. Zheng, Deterministic Entanglement Swapping in a Superconducting Circuit, *Phys. Rev. Lett.* **123**, 060502 (2019).
- [41] C. Song, K. Xu, W. Liu, C.-p. Yang, S.-B. Zheng, H. Deng, Q. Xie, K. Huang, Q. Guo, L. Zhang, P. Zhang, D. Xu, D. Zheng, X. Zhu, H. Wang, Y.-A. Chen, C.-Y. Lu, S. Han, and J.-W. Pan, 10-Qubit Entanglement and Parallel Logic Operations with a Superconducting Circuit, *Phys. Rev. Lett.* **119**, 180511 (2017).
- [42] Q.-X. Mei, B.-W. Li, Y.-K. Wu, M.-L. Cai, Y. Wang, L. Yao, Z.-C. Zhou, and L.-M. Duan, Experimental Realization of the Rabi-Hubbard Model with Trapped Ions, *Phys. Rev. Lett.* **128**, 160504 (2022).
- [43] D. M. Meekhof, C. Monroe, B. E. King, W. M. Itano, and D. J. Wineland, Generation of Nonclassical Motional States of a Trapped Atom, *Phys. Rev. Lett.* **76**, 1796 (1996).
- [44] D. Leibfried, R. Blatt, C. Monroe, and D. Wineland, Quantum dynamics of single trapped ions, *Rev. Mod. Phys.* **75**, 281 (2003).
- [45] D. Lv, S. An, Z. Liu, J.-N. Zhang, J. S. Pedernales, L. Lamata, E. Solano, and K. Kim, Quantum Simulation of the Quantum Rabi Model in a Trapped Ion, *Phys. Rev. X* **8**, 021027 (2018).
- [46] M. Grant and S. Boyd, Cvx: Matlab software for disciplined convex programming, version 2.0 beta, <http://cvxr.com/cvx> (2013).
- [47] G. Vidal and R. F. Werner, Computable measure of entanglement, *Phys. Rev. A* **65**, 032314 (2002).
- [48] W. P. Schleich, *Quantum Optics in Phase Space* (Wiley, Berlin, 2001).
- [49] M. Tavis and F. W. Cummings, Exact solution for an N -molecule-radiation-field Hamiltonian, *Phys. Rev.* **170**, 379 (1968).
- [50] C. Song, K. Xu, H. Li, Y.-R. Zhang, X. Zhang, W. Liu, Q. Guo, Z. Wang, W. Ren, J. Hao, H. Feng, H. Fan, D. Zheng, D.-W. Wang, H. Wang, and S.-Y. Zhu, Generation of multicomponent atomic Schrödinger cat states of up to 20 qubits, *Science* **365**, 574 (2019).
- [51] C. Emary and T. Brandes, Quantum Chaos Triggered by Precursors of a Quantum Phase Transition: The Dicke Model, *Phys. Rev. Lett.* **90**, 044101 (2003).
- [52] R. Gutiérrez-Jáuregui and G. S. Agarwal, Probing the spectrum of the Jaynes-Cummings-Rabi model by its isomorphism to an atom inside a parametric amplifier cavity, *Phys. Rev. A* **103**, 023714 (2021).
- [53] M. Hofheinz, H. Wang, M. Ansmann, R. C. Bialczak, E. Lucero, M. Neeley, A. D. O’Connell, D. Sank, J. Wenner, J. M. Martinis, and A. N. Cleland, Synthesizing arbitrary quantum states in a superconducting resonator, *Nature (London)* **459**, 546 (2009).
- [54] S. Wallentowitz, R. L. de Matos Filho, and W. Vogel, Determination of entangled quantum states of a trapped atom, *Phys. Rev. A* **56**, 1205 (1997).
- [55] M. Soriente, T. Donner, R. Chitra, and O. Zilberberg, Dissipation-Induced Anomalous Multicritical Phenomena, *Phys. Rev. Lett.* **120**, 183603 (2018).
- [56] S. Deléglise, I. Dotsenko, C. Sayrin, J. Bernu, M. Brune, J.-M. Raimond, and S. Haroche, Reconstruction of non-classical cavity field states with snapshots of their decoherence, *Nature (London)* **455**, 510 (2008).
- [57] M.-J. Hwang and M. B. Plenio, Quantum Phase Transition in the Finite Jaynes-Cummings Lattice Systems, *Phys. Rev. Lett.* **117**, 123602 (2016).
- [58] S. Sachdev, *Quantum Phase Transitions*, 2nd ed. (Cambridge University Press, Cambridge, England, 2011).
- [59] R. Horodecki, P. Horodecki, M. Horodecki, and K. Horodecki, Quantum entanglement, *Rev. Mod. Phys.* **81**, 865 (2009).